Progress In Electromagnetics Research, Vol. 164, 109–118, 2019

Broadband Plasmonic Circuitry Enabled by Channel Domino Spoof Plasmons

Liangliang Liu[1, 2, 3, 5, *], Li Ran[1], Huadong Guo[1], Xinlei Chen[1, 2, 4], and Zhuo Li[4,*]

Abstract—Building of compact plasmonic integrated circuits based on domino spoof plasmons (DSPs) is an important requirement and still a challenge. In this work, we report the first demonstration of two kinds of channel domino plasmonic circuitries, which consist of an easy-to-manufacture periodic chain of metallic box-shaped elements inside two finite metallic plates. We reveal that only the channel DSPs itself rather than the hybrid TE_{10} and DSPs modes is supported in the part of the channel domino plasmonic waveguide with or without the metallic vias on both sides. Two channel domino plasmonic filters based on the efficient transition structures are designed, and the simulated S-parameters and near electric field distributions show excellent transmission performance in broadband. Utilizing the lateral insensitive property of these two channel DSPs, two kinds of broadband plasmonic power dividers/combiners are firstly implemented. Excellent transmission performance validates our optimizations and indicates that the proposed scheme can be easily extended to other bands. This work provides a new route for construction of deep-subwavelength DSP devices in application of high integration of microwave and terahertz circuits.

1. INTRODUCTION

Surface plasmon polaritons (SPPs) are surface electromagnetic (EM) mode propagating on the interface between metal and dielectric in the optical regime [1–3]. However, in low frequencies [e.g., microwave and terahertz (THz) regimes], metals behave as perfect electric conductors, which cannot support SPP modes. To address it, a method of etching metal surface with periodic grooves or holes has been proposed and experimentally verified in the past decade to support spoof SPPs when being textured at the subwavelength scale [4–6]. The unique ability of these spoof SPPs to mimic optical-frequency SPPs at much lower frequencies has opened novel routes for wave control at far-IR, THz, and microwave and arouses a research boom. More importantly, their physical properties can be engineered at will by tuning the geometrical parameters [7–17]. Recently, the versatility of these concepts has been substantially extended with the demonstration of a novel class of geometry-induced modes supported by an easy-to-manufacture periodic chain of metallic box-shaped elements protruding out of a metallic surface [the so-called domino spoof plasmons (DSPs)] [18–21]. The dispersion relation of the DSP modes is rather insensitive to the waveguide lateral width, preserving tight confinement and reasonable absorption loss even when the waveguide transverse dimensions are in the subwavelength regime. This property enables the simple implementation of key devices, such as tapers [22] and power dividers [18, 23]. Additionally, directional couplers [18, 20, 23, 24], waveguide bends [25], and ring resonators [18] are characterized,

Received 5 December 2018, Accepted 23 January 2019, Scheduled 19 March 2019

* Corresponding author: Liangliang Liu (llliu@nuist.edu.cn).

[1] Jiangsu Key Laboratory of Meteorological Observation and Information Processing, Nanjing University of Information Science and Technology (NUIST), Nanjing, China, 210044. [2] Collaborative Innovation Center of Atmospheric Environment and Equipment Technology, NUIST, Nanjing, China, 210044. [3] Key Laboratory of Dynamic Cognitive System of Electromagnetic Spectrum Space (Nanjing Univ. Aeronaut. Astronaut.), Ministry of Industry and Information Technology, Nanjing, China, 211106. [4] Key Laboratory of Radar Imaging and Microwave Photonics, Ministry of Education, College of Electronic and Information Engineering, NUAA, Nanjing, China, 211106. [5] State Key Laboratory of Millimeter Waves, Southeast University, Nanjing, China, 210096.

demonstrating the flexibility of the DSPs, and their inherent design advantages (including deep-subwavelength confinement, low bending losses, and broadband operation [26–31]) are bringing closer the prospect of developing practical surface plasmonic circuitry for microwave and THz applications requiring high integration density.

Within general endeavor, the building of compact plasmonic integrated circuits would stand out as an important accomplishment. This requires the design of plasmonic waveguides carrying tightly confined electromagnetic modes, preferably with subwavelength transverse cross section. Recently, a hybrid spoof SPPs has been put forward, which is composed of periodically rectangular air square grooves [32, 33] or holes [34] etched on the metal surface of one side of the substrate integrated waveguide (SIW, which is a common transmission line in the high-performance microwave or millimeter wave planar components and circuits) or a series of metallic vias with finite depth [35] inside the SIW to mimic a box-shaped elements of the traditional DSPs. Nevertheless, the most outstanding property of the DSPs that the dispersion relation is insensitive [18–31] to the waveguide transverse dimension cannot be achieved.

In this work, we report two classes of channel domino plasmonic functional devices, which consist of periodical metallic box-shaped elements inside a SIW with or without two-side metallic vias. Two optimized transition structures composed of two tapered SIWs connected by a channel domino array with gradient heights and lateral widths are designed to realize high efficiency and broadband conversion between the conventional TE_{10} guided waves and the channel DSPs, respectively. Two broadband plasmonic filters based on the efficient transition structures are designed, and the simulated S-parameters and near electric field distributions show excellent transmission performance in broadband. On the other hand, utilizing the lateral insensitive property of these two channel DSPs, two broadband plasmonic power dividers/combiners are implemented. Excellent transmission performance validates our optimizations and indicates that the proposed scheme can be extended to other bands, and these results provide a new insight application of the DSPs in the high integration of microwave or THz circuits with plasmonic devices [36–38].

2. DISPERSION PROPERTIES OF CHANNEL DOMINO SPOOF PLASMONS

The basic properties of the channel DSPs are described with the dispersion characteristics, which are essential in the momentum matching for the design of broadband plasmonic circuitry. As we know, a periodical domino metallic block array attached on a metal plate shown in Fig. 1(a) can support the propagation of the so-called DSPs [15, 16], in which the domino array periodicity is d, and the domino height and lateral width are denoted by h and w, respectively. The interval between two adjacent domino metallic blocks is denoted as a. When the transverse magnetic (TM) polarized waves propagate along the x direction, only the fundamental surface mode is considered. An approximation for the dispersion relation of the DSPs in the limit $w \to \infty$, neglecting the diffraction effects and for $\lambda \gg d, a$ (λ is the operation wavelength), can be expressed as $k_x = k_0\sqrt{1+\frac{a^2}{d^2}tan^2(q_y h)}$, where k_x is the modal wave vector along x direction; $k_0 = 2\pi/\lambda$ is the wave vector in free space; and the y component of the wave vector inside the grooves, q_y, is related to the corresponding x and z components by $q_x^2 + q_y^2 + q_z^2 = k_0^2$. The EM fields inside the grooves are independent of x and z for the chosen longitudinal polarization and thus q_x=$q_z = 0$, q_y=k_0. This means that the dispersion of the DSPs presents an asymptote for $k_0 h = \pi/2$, and when $0 < k_0 h < \pi/2$, k_x will be a real number and $k_x > k_0$.

As shown in Figs. 1(b) and 1(c), different from the traditional DSPs in Fig. 1(a), the channel DSP modes will be supported by the periodical domino metallic blocks attached between two infinite metallic plates and denoted by Case I without two-side metallic vias and Case II with metallic vias. Firstly, to understand the difference of the basic EM property for the traditional and channel DSPs, we obtained simulated dispersion curves by the eigenmode solver of the commercial software CST Microwave Studio and plotted them in Fig. 1(d). For the sake of clarity, the dispersion curves with varying height h ($h = p$, $1.5p$, $1.8p$) are obtained. It is shown that the asymptotic frequency is mainly controlled by domino height h when other parameters are fixed. Within the propagation band, as h increases, the dispersion curve of the channel DSPs deviates more away from the light line than that of the traditional DSPs, indicating a stronger confinement characteristic and lower cut-off frequency of the channel DSPs than that of the traditional DSPs. The dispersion evolution of the channel DSPs can be used to design

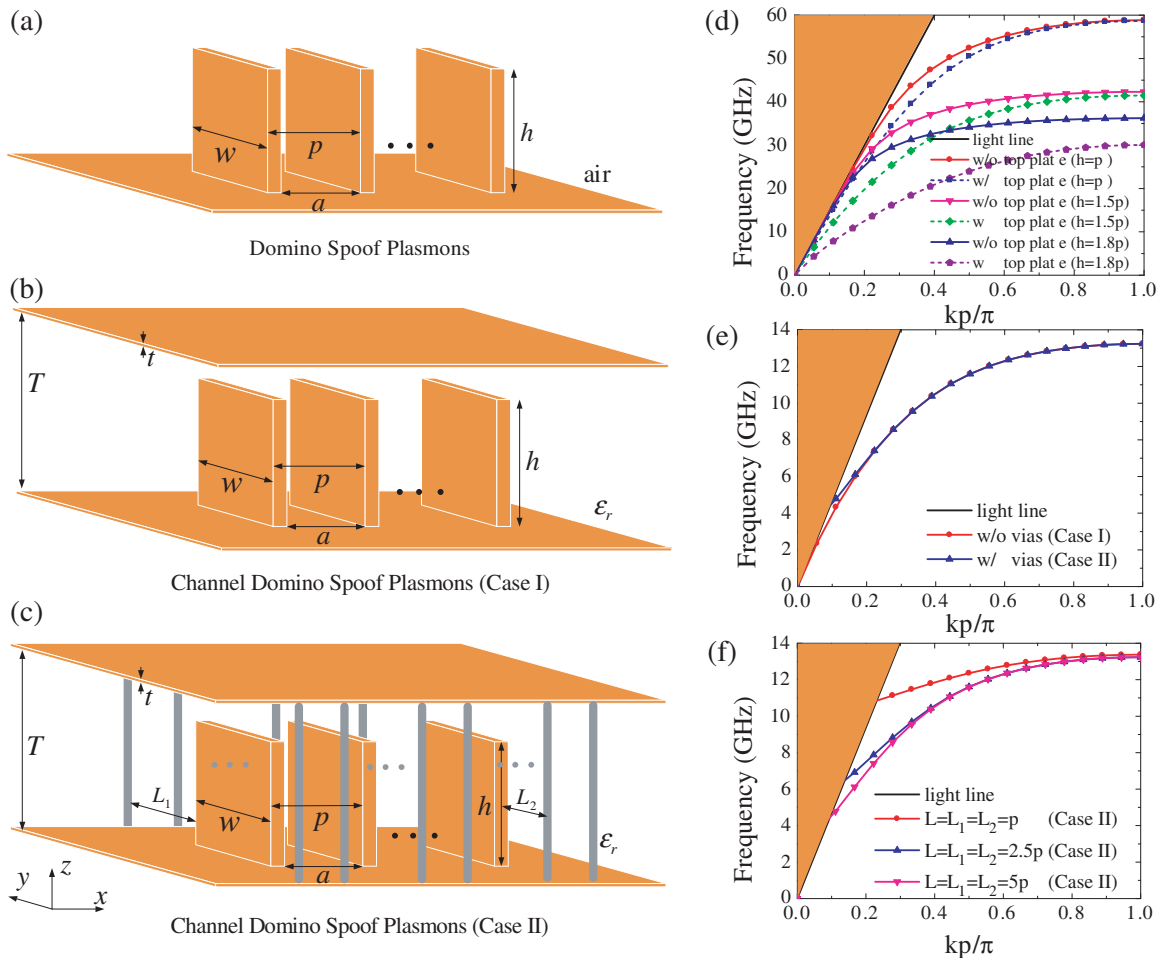

Figure 1. (a) Schematic drawing of the periodical box-shaped domino array etched on a infinite metallic plate to support the traditional DSPs. (b) and (c) Schematic drawing of the channel periodical domino array inside two finite metallic plate without (Case I) or with (Case II) metallic vias,respectively. (d) Dispersion curves of the DSPs and the channel DSPs (Case I) with varying metallic block height h, where $p = 1\,\text{mm}$, $a = 0.5p$, $w = 4p$, $T = 1.9p$, $t = 0.018p$ and ε_r=1. (e) Dispersion curves of the channel DSPs with (Case II) or without (Case I) two-side metallic vias. (f) Dispersion curves of the channel DSPs (Case II) with varying interval L ($L = L_1 = L_2$) between the metallic block and the via.

some efficient functional devices such as the broadband plasmonic filter later by optimizing the gradient domino height.

Secondly, to demonstrate the difference between these two channel DSPs, the dispersion curves of Case I and Case II are obtained and shown in Figs. 1(e) and 1(f). We observe that the surface EM modes supported by these two cases are almost coincident, except for the low frequency region. In the low frequency, the cutoff frequency of Case II is higher than that of Case I (see Fig. 1(e)), which may be caused by the coupling between the metallic via and domino metallic block. As expected, as interval L increases ($L = L_1 = L_2 = p$, $2.5p$, $5p$, see Fig. 1(f)), the low cutoff frequency of Case II gradually decreases, indicating that the coupling between the metallic via and the domino metallic block is gradually weakened as L gradually increases.

Moreover, the most intriguing characteristic of the DSPs is their dispersion in insensitive to the lateral width w. As shown in Figs. 2(a) and 2(b), we obtained dispersion curves of these two cases with varying lateral width w ($w = 0.1p$, $0.5p$, p, $5p$, $10p$) when other parameters are fixed. It is obvious that the dispersion curves of these two cases are both insensitive to the variation of lateral dimension w. The described behavior shows that when the lateral size of the structure supporting such modes becomes

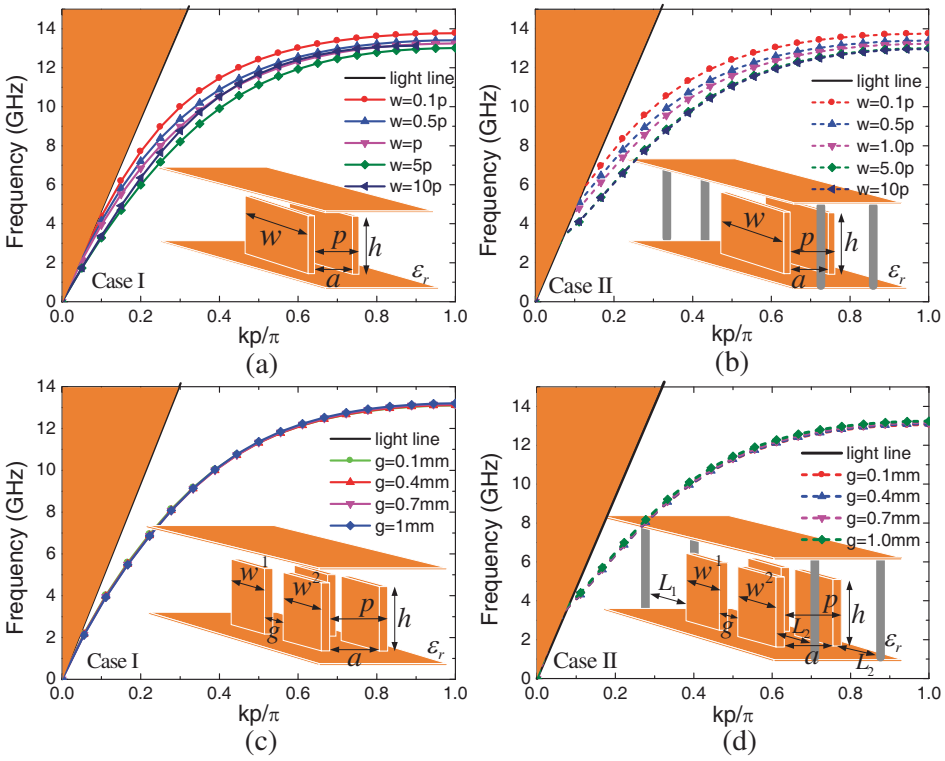

Figure 2. (a) and (b) Dispersion curves of the two Cases with varying lateral width w of the metallic blocks without two-side metallic vias and with metallic vias, respectively. (c) and (d) Dispersion curves of two Cases with varying interval g between two split metallic blocks without two-side metallic vias and with metallic vias, respectively.

subwavelength, either the modal size grows, or the effective index increases. A stripe of large lateral width essentially supports an SPP mode, but as this width is decreased and becomes subwavelength, the plasmonic modes that are not cutoff become either highly confined but quite lossy, or otherwise highly delocalized. The insensitivity of these two channel DSPs to the lateral dimension, which constitutes the foundation of some of the devices such as the power divider/combiner later, can be linked in an intuitive way to the structure geometry.

3. BROADBAND AND HIGH-EFFICIENCY CHANNEL DOMINO PLASMONIC BAND-PASS FILTER

According to the aforementioned two channel DSPs, as shown in Figs. 3(a) and 3(b), we design two band-pass channel domino plasmonic filters by utilizing the high-pass and low-pass characteristics of the SIW and channel DSPs, respectively. Each channel domino plasmonic filter is divided into three regions. Region I of two cases is a transition part between the conductor-backed coplanar waveguide and SIW [39–41]. Region III is the proposed channel domino plasmonic waveguide with a periodic domino array in the x direction. It is obviously seen that the main difference between the two cases is that Regions III of Case I have no metallic vias on both sides, whereas Case II is in contrast. Hence, for Region II of Case I, we need to ensure the efficient conversion between the SIW and the pure channel domino plasmonic waveguide with a gradient domino height varying from h_1 to h_m (see Fig. 3(d)) to realize smooth momentum and impedance matching between them. On the other hand, a taper with gradient domino lateral width varies from w_1 to w_n (see Fig. 3(c)), and a flaring curve consists of a series of metallic vias with angle degree of θ (it is remarked that the flaring curve can be different [29-31]) which need to be simultaneously introduced to avoid the transverse energy leakage of the surface EM waves.

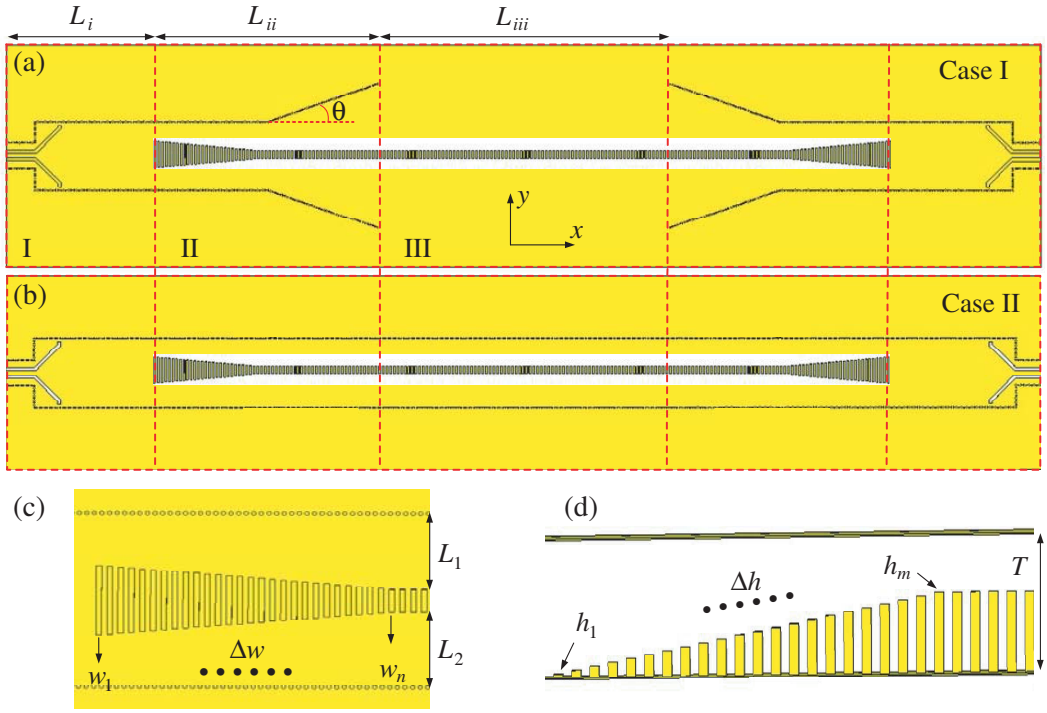

Figure 3. (a) and (b) The schematic configuration of the two channel domino plasmonic filters with the cross-section in the xy plane, in which each plasmonic filter is divided into three regions, and the Regions I, II and III correspond to a transition part between the conductor-backed coplanar waveguide and the SIW, an efficient conversion part between the SIW and the channel domino plasmonic waveguide, and the channel domino plasmonic waveguide itself, respectively. (c) and (d) The gradient domino lateral width w varies from w_1 to w_n with a step of Δw and the domino height h varies from h_1 to h_m with a step of Δh in Region II of the two Cases, respectively.

However, the second requirement is not needed in Case II due to the EM field confinement of the SIW with two-side metallic vias. In the SIW part, we only consider TE_{10} mode as the dominant excitation, whose magnetic field has only x and y components, so as to excite the channel DSPs propagating on the surface of the domino array. Through the above designs, the conventional TE_{10} wave supported in the SIW can be efficiently converted into the channel DSPs and only the channel DSPs itself is supported in Region III of both cases rather than their hybrid modes.

To obtain a broadband and high-efficiency channel domino plasmonic filter, we adopted the optimization scheme in [29–31]. After a series of optimized designs and simulations, two optimal hybrid plasmonic filters are achieved. The length of each region is optimized as $L_i = 20\,\text{mm}$, $L_{ii} = 22\,\text{mm}$, $L_{iii} = 56\,\text{mm}$. In Region I, a common SIW with cutoff frequency of $f_{c1} = 4.75\,\text{GHz}$ is employed (for the SIW, the diameter of the metallic via is 0.2 mm, and the interval between two adjacent vias is 0.35 mm along x direction and 10 mm along y direction, thus the operating frequency of the SIW can be obtained by Equation (9) in [41]), and the corresponding S-parameters are shown as the solid lines in Fig. 4(b). In Region III, the period $p = 1.25\,\text{mm}$, interval $a = 0.625\,\text{mm}$, height $h = 1.76$ mm, lateral width $w = 1\,\text{mm}$, and the dispersion curves are displayed as the red solid (Case I) and blue dotted (Case II) lines in Fig. 4(a) with the upper cutoff frequency $f_{c2} = 9.6\,\text{GHz}$. We remark that the dimensions of the domino array are cautiously chosen so as to ensure that the operation frequency of channel DSPs is in the fundamental mode band of the SIW. Otherwise, the transition performance will be deteriorated since the electric field intensity distribution for the high-order modes of the SIW in the cross section may lead to inefficient field confinement of the DSPs. More importantly, the lateral decay lengths δ_d (δ_d is defined as the lateral distance of the DSPs away from the surface of the domino plasmonic waveguide when the magnitude of its surface electric field in the lateral space decays to e^{-1} times of the original's,

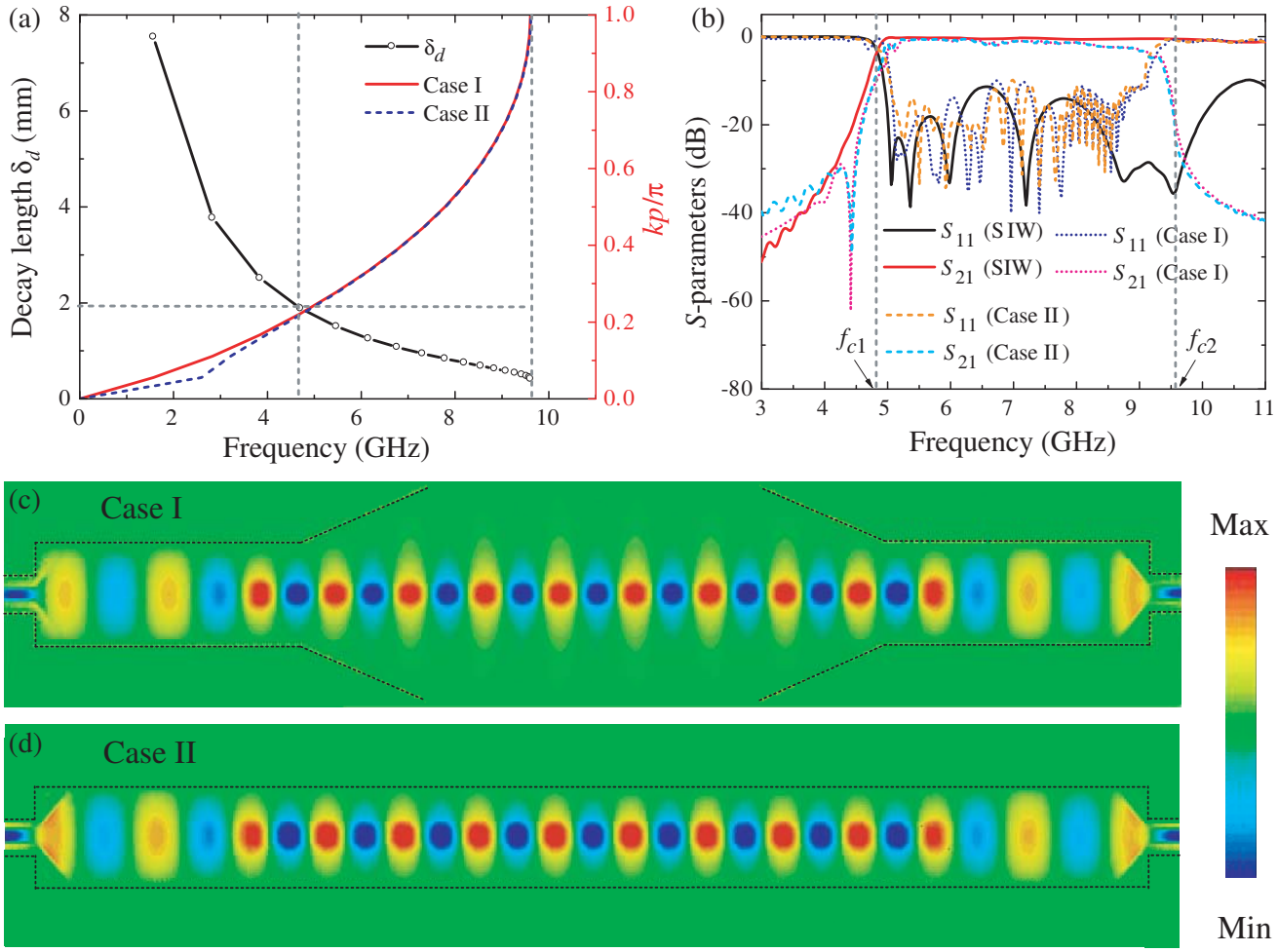

Figure 4. (a) The dispersion curves and the corresponding lateral decay lengths of the two channel DSPs in Region III, where the material of Rogers 6010 ($\varepsilon_r = 10.2$, $\tan\delta = 0.0023$) is chosen as the dielectric substrate with thickness $T = 1.905$ mm. (b) The simulated S-parameters of the SIW, Cases I and II, respectively. (c) and (d) The simulated near-field distributions (E_z component, V/m) of the two channel DSPs at 9 GHz on the xy plane slightly 0.1 mm above the domino array.

e.g., $|\mathbf{E}|e^{-k_y\delta_d} = |\mathbf{E}|e^{-1}$ [31], $k_y = \sqrt{k_x^2 - \varepsilon_r k_0^2}$ and ε_r is the relative permittivity of the medium around the domino plasmonic waveguide) of these two DSPs in Region III are donated as black line in Fig. 4(a). As expected, the lateral decay lengths of both two DSPs are less than 2 mm in the whole operation frequency band from f_{c1} to f_{c2}, which ensure efficient transmission of the DSPs on the surface of the domino array with or without the two-side metallic vias. In Region II, a transition taper with gradient domino height h varies from $h_1 = 0.09$ mm to $h_{19} = 1.76$ mm with a step of $\Delta h = 0.09$ mm, and gradient domino lateral width w varies from $w_1 = 4$ mm to $w_{19} = 1.3$ mm with a step of $\Delta w = 0.05$ mm, as well as $\theta = 30^\circ$ for Case I.

To quantitatively characterize the two plasmonic filters, their corresponding S-parameters are obtained and shown in Fig. 4(b), in which S_{11} is less than -10 dB from 5 GHz to 9 GHz, and S_{21} is higher than -0.5 dB from 5 GHz to 9 GHz, indicating an efficient transmission performance of these two plasmonic filters in broadband. As expected above, we observe that the S-parameter curves of the two plasmonic filters agree well with each other, verifying our aforementioned discussions in Section 2. In addition, in order to visually demonstrate the efficient transmission performance of the two plasmonic filters, we plot in Figs. 4(c) and 4(d) the near-field distributions of the two plasmonic filters at 9 GHz on the xy plane which is 0.1 mm away from the surface of the domino array. The gradually increasing

surface electric field intensity distribution clearly shows how the transitional TE_{10} guided waves are smoothly converted into the DSPs and tightly confined on the surface of the domino array.

4. BROADBAND CHANNEL DOMINO PLASMONIC POWER DIVIDER/COMBINER

Figs. 2(a) and 2(b) show that the dispersion relations of the proposed two channel DSPs are both rather insensitive to the waveguide width, which preserve tight confinement and reasonable absorption loss even when the waveguide transverse dimension is far below the subwavelength scale. This property enables the simple implementation of some key devices, such as tapers and power dividers/combiners. Moreover, flexibility and high-efficiency of the transition structure allow us to design a variety of efficient functional devices for microwave and THz applications [8–17]. In this work, a plasmonic power divider/combiner shown in Fig. 5(a) is proposed and easily built, where the width of the domino array in Region III is $w = 1.3\,\text{mm}$, $w^1 = w^2 = 0.6\,\text{mm}$, the interval $g = 0.1\,\text{mm}$ [see the inset in Fig. 5(a)], and other parameters are the same as that in Fig. 3(a). The radii and angles of two bending arc lines are $r = 18\,\text{mm}$ (as discussed in [18], the greater the radius is, the lower the loss is). As shown in Fig. 5(a), the simulated near-field distributions (E_z component) of Case I are slightly 0.1 mm above the domino array at 9 GHz which is plotted on the xy plane. We observe that a single DSP mode on a wide domino array (input chain 1) is split into two arms (output chains 2 and 3), and the total loss is mainly generated in the bend region [18–31]. In Fig. 5(b), the simulated S_{11}, S_{22} and S_{33} are all lower than $-10\,\text{dB}$ from

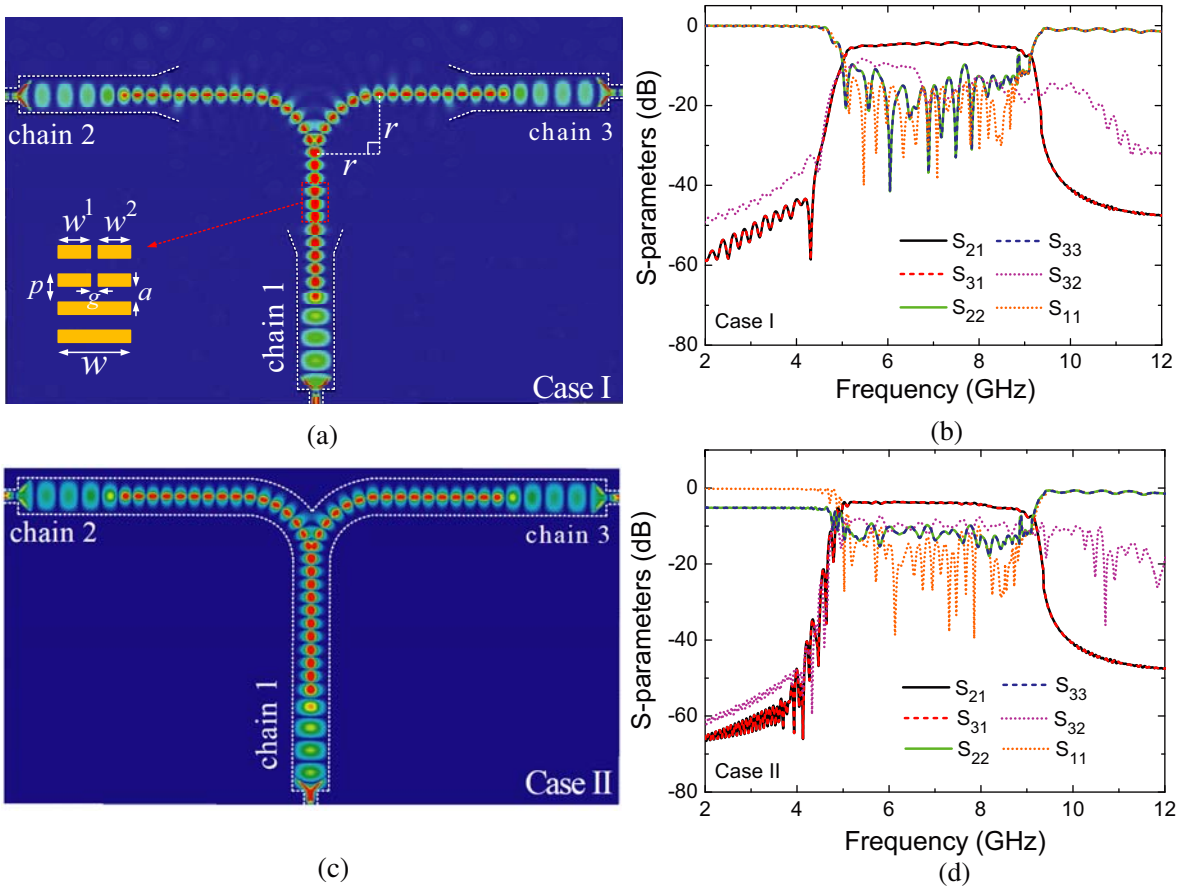

Figure 5. Two kinds of domino plasmonic power divider/combiner. (a) and (b) are the cross-section of simulation model and the simulated near-field distributions of E_z component (V/m) at 9 GHz on the xy plane for Case I, respectively. (c) and (d) are the cross-section of simulation model and the simulated near-field distributions of E_z component (V/m) at 9 GHz on the xy plane for Case II, respectively.

5 GHz to 9 GHz, indicating an efficient conversion between the SIW and domino plasmonic waveguide. Moreover, S_{21} and S_{31} are the same and more than -4.3 dB from 5 GHz to 9 GHz, which show that the input power on chain 1 is equally divided into two output powers on chains 2 and 3, respectively. In addition, a good isolation between chains 2 and 3 shown as S_{32} below -14 dB is achieved in the whole band. For comparison, the surface electric field distributions and simulated S-parameters of the second domino plasmonic power divider/combiner are obtained and shown in Figs. 5(c) and 5(d), respectively. These results highlight that two efficient double chains broadband plasmonic power dividers (or the vice versa, i.e., power combiner) are achieved, and we believe that n-chain ones can be similarly designed based on the insensitive dispersion property of the DSPs.

5. CONCLUSION

In summary, we have presented two channel DSPs supported by a periodic chain of metallic box-shaped blocks inside two finite metallic plates. Two optimize transition structures to realize the high-efficiency and broadband mode conversion are proposed respectively. The transition structure consists of two tapered SIWs connected by a channel domino array with gradient heights and lateral widths. Two efficient and broadband plasmonic filters based on the efficient transition scheme are designed, and two broadband plasmonic power dividers/combiners based on the lateral insensitive property of the channel DSPs are implemented. These results indicate that the channel DSPs can find a variety of applications in the integration of conventional microwave or THz circuits with plasmonic devices.

ACKNOWLEDGMENT

This work was supported in part by the National Natural Science Foundation of China (No. 61701246), the Natural Science Foundation of Jiangsu Higher Education Institutions of China (No. 17KJB140014), the State Key Laboratory of Millimeter Waves, Southeast University, China (No. K201924), the Key Laboratory of Dynamic Cognitive System of Electromagnetic Spectrum Space (Nanjing Univ. Aeronaut. Astronaut.), Ministry of Industry and Information Technology, China (No. KF20181909), Jiangsu Key Laboratory of Meteorological Observation and Information Processing Open Project (No. KDXS1802), and the Priority Academic Program Development of Jiangsu Higher Education Institutions. Z. Li acknowledges the financial support from National Natural Science Foundation of China under Grant No. 61871215, Six talent peaks project in Jiangsu Province under Grant No. 2018-GDZB-009 and Foundation of Key Laboratory of Radar Imaging and Microwave Photonics, NUAA, Ministry of Education under Grant No. XCA17001-05.

REFERENCES

1. Barnes, W. L., A. Dereux, and T. W. Ebbesen, "Surface plasmon subwavelength optics," *Nature* Vol. 424, No. 6950, 824–830, 2003.
2. Maier, S. A., *Plasmonics: Fundamentals and Applications* , Springer, New York, 2007.
3. Pitarke, J. M., V. M. Silkin, E. V. Chulkov, and P. M. Echenique, "Theory of surface plasmons and surface-plasmon polaritons," *Rep. Prog. Phys.*, Vol. 70, No. 1, 1, 2006.
4. Pendry, J. B., L. Martin-Moreno, and F. J. Garcia-Vidal, "Mimicking Surface Plasmons with Structured Surfaces," *Science*, Vol. 305, No. 5685, 847–848, 2004.
5. Garcia-Vidal, F. J., L. Martin-Moreno, and J. B. Pendry, "Surfaces with holes in them: New plasmonic metamaterials," *J. Opt. A, Pure Appl. Opt.*, Vol. 7, No. 2, S97–S101, 2005.
6. Hibbins, A. P., B. R. Evans, and J. R. Sambles, "Experimental verification of designer surface plasmons," *Science*, Vol. 308, No. 5722, 670–672, 2005.
7. Williams, C. R., S. R. Andrews, S. A. Maier, A. I. Fernandez-Dominguez, L. Martin-Moreno, and F. J. Garcia-Vidal, "Highly confined guiding of terahertz surface plasmon polaritons on structured metal surfaces," *Nat. Photon.*, Vol. 2, No. 3, 175–179, 2008.

8. Liu, L. L., Z. Li, C. Q. Gu, P. P. Ning, B. Z. Xu, Z. Y. Niu, and Y. J. Zhao, "Multi-channel composite spoof surface plasmon polaritons propagating along periodically corrugated metallic thin films," *J. Appl. Phys.*, Vol. 116, No. 1, 013501, 2014.
9. Wu, J. J., "Subwavelength microwave guiding by periodically corrugated strip line," *Progress In Electromagnetics Research*, Vol. 104, 113–123, 2010.
10. Liao, Z., J. Zhao, B. C. Pan, X. P. Shen, and T. J. Cui, "Broadband transition between microstrip line and conformal surface plasmon waveguide," *J. Phys. D. Appl. Phys.*, Vol. 47, No. 31, 315103, 2014.
11. Ma, H. F., X. P. Shen, Q. Cheng, W. X. Jiang, and T. J. Cui, "Broadband and high-efficiency conversion from guided waves to spoof surface plasmon polaritons," *Laser Photon. Rev.*, Vol. 8, No. 1, 146–151, 2014.
12. Liu, L. L., Z. Li, B. Z. Xu, P. P. Ning, C. Chen, J. Xu, X. L. Chen, and C. Q., Gu, "Dual-band trapping of spoof surface plasmon polaritons and negative group velocity realization through microstrip line with gradient holes," *Appl. Phys. Lett.*, Vol. 107, No. 20, 201602, 2015.
13. Cui, T. J., "Microwave metamaterials-from passive to digital and programmable controls of electromagnetic waves," *J. opt.*, Vol. 19, No. 4, 2017.
14. Cui, T. J., "Microwave metamaterials," *National Sci. Rev.*, Vol. 5, No. 2, 134–136, 2018.
15. Zhou, Y. J. and B. J. Yang, "Planar spoof plasmonic ultra-wideband filter based on low-loss and compact terahertz waveguide corrugated with dumbbell grooves," *Appl. Opt.*, Vol. 54, No. 14, 4529–4533, 2015.
16. Zhang, H. C., Y. F. Fan, J. Guo, X. J. Fu, and T. J. Cui, "Second-harmonic generation of spoof surface plasmon polaritons using nonlinear plasmonic metamaterials," *ACS Photon.*, Vol. 3, No. 1, 139–146, 2016.
17. Liu, L. L., L. Wu, J. J. Zhang, Z. Li, B. L. Zhang, and Y. Luo, "Backward Phase Matching for Second Harmonic Generation in Negative-Index Conformal Surface Plasmonic Metamaterials," *Adv. Sci.*, 1800661, 2018.
18. Martin-Cano, D., M. L. Nesterov, A. I. Fernandez-Dominguez, F. J.Garcia-Vidal, L. Martin-Moreno, and E. Moreno, "Domino plasmons for subwavelength terahertz circuitry," *Opt. Express*, Vol. 18, 754–764, 2010.
19. Nesterov, M. L., D. Martin-Cano, A. I. Fernandez-Dominguez, E.Moreno, L. Martin-Moreno, and F. J. Garcia-Vidal, "Geometrically induced modification of surface plasmons in the optical and telecom regimes," *Opt. Lett.*, Vol. 35, No. 3, 517–520, 2010.
20. Zhao, W. S., O. M. Eldaiki, R. X. Yang, and Z. L. Lu, "Deep subwavelength waveguiding and focusing based on designer surface plasmons," *Opt. Express*, Vol. 18, No. 20, 21498–21503, 2010.
21. Brock, E. M. G., E. Hendry, and A. P. Hibbins, "Subwavelength lateral confinement of microwave surface waves," *Appl. Phys. Lett.*, Vol. 99, 051108, 2011.
22. Cano, D. M., O. Q. Teruel, E. Moreno, L. Martin-Moreno, F. J.Garcia-Vidal, "Waveguided spoof surface plasmons with deep-subwavelength lateral confinement," *Opt. Lett.*, Vol. 36, No. 23, 4635–4637, 2011.
23. Ma, Y. G., L. Lan, S. M. Zhong, and C. K. Ong, "Experimental demonstration of subwavelength domino plasmon devices for compact high frequency circuit," *Opt. Express*, Vol. 19, 189–198, 2011.
24. Boroujeni, M. A., K. Altmann, B. Scherger, C., Jansen, M. Shahabadi, and M. Koch, "Terahertz Parallel-Plate Ladder Waveguide With Highly Confined Guided Modes," *IEEE Trans. Terahertz Science and Tech.*, Vol. 3, No. 1, 87–95, 2013.
25. Kumar, G., S. S. Li, M. M. Jadidi, and T. E. Murphy, "Terahertz surface plasmon waveguide based on a one-dimensional array of silicon pillars," *New J. Phys.*, Vol. 15, 085031, 2013.
26. Wu, J. J., H. E. Lin, T. J. Yang, Y.-H. Kao, H.-L. Chiueh, and D. J. Hou, "Open waveguide based on low frequency spoof surface plasmon polaritons," *Journal of Electromagnetic Waves and Applications*, Vol. 5, 58–62, 2013.
27. Teruel, O. Q., "Controlled radiation from dielectric slabs over spoof surface plasmon waveguides," *Progress In Electromagnetics Research*, Vol. 140, 169–179, 2013.

28. Woolf, D., M. A. Kats, and F. Capasso, "Spoof surface plasmon waveguide forces," *Opt. Lett.*, Vol. 39, No. 3, 517–520, 2014.
29. Liu, L. L., Z. Li, B. Z. Xu, J. Yan, P. P. Ning, and C. Q. Gu, "A high-efficiency rectangular waveguide to Domino plasmonic waveguide converter in X-band," *2014 3rd IEEE Asia-Pacific Conference on Antennas and Propagation (APCAP)*, 974–977, July 2014.
30. Liu, L. L., Z. Li, B. Z. Xu, C. Q. Gu, C. Chen, P. P. Ning, J. Yan, and X. Y. Chen, "High-efficiency transition between rectangular waveguide and domino plasmonic waveguide," *AIP Adv.*, Vol. 5, No. 2, 027105, 2015.
31. Liu, L. L., Z. Li, B. Z. Xu, C. Q. Gu, X. L. Chen, H. Y. Sun, Y. J.Zhou, Q. Qing, P. Shum, and Y. Luo, "Ultra-low-loss high-contrast gratings based spoof surface plasmonic waveguide," *IEEE Trans. on Micro. Theory and Tech.*, Vol. 65, No. 6, 2008–2018,2017.
32. Zhang, Q., H. C. Zhang, H. Wu, and T. J. Cui, "A hybrid circuit for spoof surface plasmons and spatial waveguide modes to reach controllable band-pass filters," *Sci. Rep.*, Vol. 5, 16531, 2015.
33. Guan, D. F., P. You, Q. Zhang, Z. B. Yang, H. W. Liu, and S. W. Yong, "Slow-wave half-mode substrate integrated waveguide using spoof surface plasmon polariton structure," *IEEE Trans. Microw. Theory Techn.*, Vol.'66, No. 6, 2946–2952, 2018.
34. Chen, P., L. P. Li, K. Yang, and Q. Chen, 'Hybrid spoof surface plasmon polariton and substrate integrated waveguide broadband bandpass filter with wide out-of-band rejection", *IEEE Micro. and Wireless Components Lett.*, Vol. 28, No. 11, 984–986, 2018.
35. Guan, D. F., P. You, Q. Zhang, K. Xiao, and S. W. Yong, "Hybrid spoof surface plasmon polariton and substrate integrated waveguide transmission line and its application in filter," *IEEE Trans. Micro. Theory Techn.*, Vol. 65, No. 12, 4925–4932, 2017.
36. Wu, Q. H., G. R. Ding, J. L. Wang, and Y. D. Yao, "Spatial-temporal opportunity detection for spectrum-heterogeneous cognitive radio networks: Two-dimensional sensing," *IEEE Trans. on Wireless Commun.*, Vol. 12, No. 2, 516–526, 2013.
37. Ding, G. R., J. L. Wang, Q. H. Wu, Y. D. Yao, F. Song, and T. A.Tsiftsis,"Cellular-base-station-assisted device-to-device communications in TV white space," *IEEE J. on Selected Areas in Commun.*, Vol. 34, No. 1, 107–121, 2016.
38. Ding, G. R., J. L. Wang, Q. H. Wu, Y. D. Yao, R. P. Li, H. G., Zhang, and Y. L. Zou, "On the limits of predictability in real-world radio spectrum state dynamics: From entropy theory to 5G spectrum sharing," *IEEE Commun. Magazine*, Vol. 53, No. 7, 178–183, 2015.
39. Chen, X. P. and K. Wu, "Low-loss ultra-wideband transition between conductor-backed coplanar waveguide and substrate integrated waveguide," *IEEE MTT-S International Microwave Symposium Digest*, 349–352, 2009.
40. Taringou, F. and J. Bornemann, "New substrate-integrated to coplanar waveguide transition," *Proceedings of the 41st European Microwave Conference*, 428–431, Manchester, UK, October 2011.
41. Xu, F. and K. Wu, "Guided-wave and leakage characteristics of substrate integrated waveguide," *IEEE Trans. on Micro. Theory and Tech.*, Vol. 53, No. 1, 66–73, 2005.